Neuro-Oncology
27(1), 167–183, 2025 | https://doi.org/10.1093/neuonc/noae169 | Advance Access date 30 August 2024

ENPP1 induces blood–brain barrier dysfunction and promotes brain metastasis formation in human epidermal growth factor receptor 2-positive breast cancer

Liliana Santos, Francesca Tomatis, Hugo R. S. Ferreira, Sara F. F. Almeida, Edward Ciputra, José Sereno, Rui Almeida, Paulo Teixeira, Ana Sofia Ribeiro, João N. Moreira, Ana P. Silva, Lino Ferreira, Antero J. Abrunhosa, and Célia M. Gomes

All author affiliations are listed at the end of the article

Corresponding Author: Célia M. Gomes, PhD, Coimbra Institute for Clinical and Biomedical Research (iCBR), Faculty of Medicine, University of Coimbra, 3000-548 Coimbra, Portugal (cgomes@fmed.uc.pt).

Abstract

Background. Brain metastasis (BrM) is a devastating end-stage neurological complication that occurs in up to 50% of human epidermal growth factor receptor 2-positive (HER2+) breast cancer (BC) patients. Understanding how disseminating tumor cells manage to cross the blood–brain barrier (BBB) is essential for developing effective preventive strategies. We identified the ecto-nucleotidase ENPP1 (ectonucleotide pyrophosphatase/phosphodiesterase 1) as specifically enriched in the secretome of HER2+ brain metastatic cells, prompting us to explore its impact on BBB dysfunction and BrM formation.

Methods. We used in vitro BBB and in vivo premetastatic mouse models to evaluate the effect of tumor-secreted ENPP1 on brain vascular permeability. BBB integrity was analyzed by real-time fluorescence imaging of 20 kDa Cy7.5-dextran extravasation and immunofluorescence staining of adherens and tight junction proteins. Pro-metastatic effects of ENPP1 were evaluated in an experimental brain metastatic model.

Results. Systemically secreted ENPP1 from primary breast tumors impaired the integrity of BBB with loss of tight and adherens junction proteins early before the onset of BrM. Mechanistically, ENPP1 induced endothelial cell dysfunction by impairing insulin signaling and its downstream AKT/GSK3β/β-catenin pathway. Genetic ablation of ENPP1 from HER2+ brain metastatic cells prevented endothelial cell dysfunction and reduced metastatic burden while prolonging the overall and metastasis-free survival of mice. Furthermore, plasmatic ENPP1 levels correlate with brain metastatic burden and inversely with overall survival.

Conclusions. We demonstrated that metastatic BC cells exploit the ENPP1 signaling for cell transmigration across the BBB and brain colonization. Our data implicate ENPP1 as a potential biomarker for poor prognosis and early detection of BrM in HER2+ BC.

Key Points

- Tumor-secreted ENPP1 increases the blood-brain barrier permeability to facilitate brain colonization.
- ENPP1 knockout prevents endothelial cell dysfunction and reduces metastatic burden.
- Systemic ENPP1 levels correlate inversely with overall survival.

Graphical Abstract

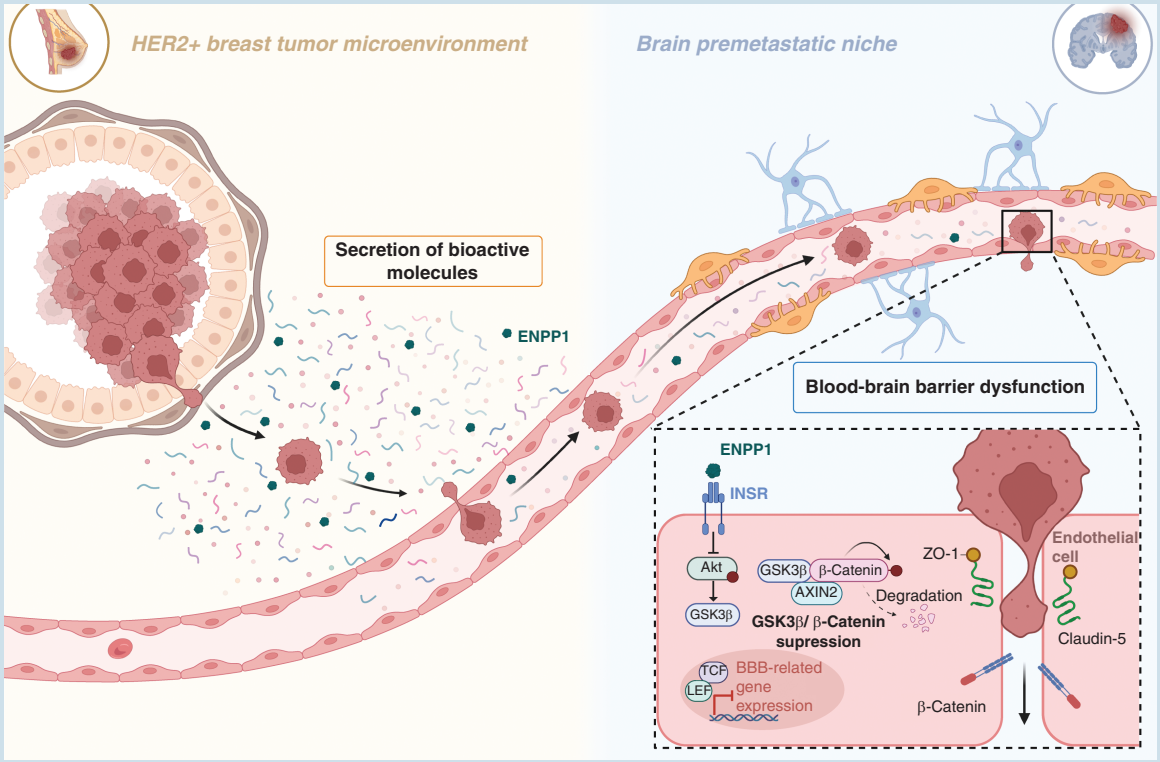

Importance of the Study

The incidence of brain metastasis (BrM) in human epidermal growth factor receptor 2-positive (HER2+) breast cancer is increasing and remains a clinical challenge associated with poor prognosis and limited therapeutic options. Recent studies have highlighted the importance of blood-brain barrier (BBB) dysfunction in the pathophysiology of BrM. Understanding how tumor cells cross the BBB provides opportunities for the development of preventive and therapeutic strategies. We have uncovered a novel mechanism by which HER2+ BC cells compromise the BBB to metastasize to the brain. We found that ENPP1 secreted by brain metastatic cells disrupts the BBB to facilitate cell extravasation. Furthermore, genetic depletion of ENPP1 prevented endothelial cell dysfunction, reduced metastatic burden, and prolonged metastasis-free survival in preclinical models. Importantly, systemic ENPP1 levels correlated with rapid metastatic progression, positioning ENPP1 as a plasma-based biomarker for BrM risk. The functional implications of ENPP1 that we have identified suggest that targeting ENPP1 may be an effective therapeutic strategy to prevent BrM relapse.

Brain metastases (BrM) represent a significant challenge in the management of solid malignancies, particularly for patients with human epidermal growth factor receptor 2-positive (HER2+) breast cancer (BC). Approximately 15%–20% of BC cases are HER2+, and up to 50% of these cases develop BrM during the disease course.[1] The current standard treatments for BrM are primarily palliative and offer limited benefits, resulting in a markedly reduced median survival time of 3–12 months and a rapid decline in quality of life.[2] This unfavorable prognosis is attributed to advancements in diagnostic techniques and systemic therapies that are effective extra-cranially but often fail to offer similar benefits within the brain.[3] Additionally, BrM can occur years to decades after the removal of the primary tumor (PT), indicating extensive biological changes during the intervening years.[4] Thus, there is an urgent need for early preventive strategies to mitigate the risk of BrM in these patients.

During BrM formation, systemic secreted factors from the PT or early disseminated tumor cells have been implicated in modifying the brain microenvironment by recruiting immune cells, activating resident astrocytes and microglia, and remodeling the extracellular matrix, thereby creating a hospitable brain premetastatic niche for cancer cell growth and survival.[5] For instance, systemic lipocalin-2 (LCN2) signaling

from the PT instigates neuroinflammation in the brain metastatic niche by activation of astrocytes, leading to the recruitment of LCN2-producing granulocytes from the bone marrow to the brain metastatic microenvironment, favoring the development of BrM.[6] Additionally, dysfunction of the blood-brain barrier (BBB) has emerged as a pivotal early event in BrM formation.[7] The BBB comprises specialized endothelial cells (ECs) with continuous tight and adherens junctions, pericytes, basement membranes, and astrocytic foot processes, collectively acting to impede the dissemination of cancer cells into the brain parenchyma.[8] While several studies have highlighted the role of tumor-secreted factors in mediating BBB dysfunction,[9,10] the early mechanisms remain elusive, as most investigations have focused on BBB impairment during brain colonization, overlooking the critical early stages preceding its development.

Therefore, our study aimed to investigate the role of secreted molecules from HER2+ BC cells in BBB dysfunction during the formation of the pre-metastatic niche before the onset of BrM. We demonstrate that systemic signaling derived from brain metastatic HER2+ PTs instigates BBB dysfunction and identifyed the enzyme ectonucleotide pyrophosphatase/phosphodiesterase 1 (ENPP1) as a primary contributor to these changes. ENPP1 has gained considerable recognition as an intrinsic regulator of the immune system.[11] Moreover, it acts as a negative regulator of the insulin signaling pathway at the receptor level, inducing insulin resistance,[12–16] a condition implicated in BBB dysfunction in neurodegenerative diseases and metabolic disorders.[17,18] Noteworthy, we further clarify that ENPP1 secreted by HER2+ brain-tropic BC cells induces BBB dysfunction by suppressing the AKT/GSK3β/β-catenin pathway downstream of the insulin receptor (INSR), resulting in decreased stability of tight and adherens junction proteins in microvascular ECs. Functionally, ENPP1 genetic depletion or pharmacological inhibition effectively reduces metastatic burden in preclinical models, highlighting its potential as a therapeutic target. Moreover, ENPP1 was detected in the plasma of mice with HER2+ metastatic breast tumors before BrM formation and correlated with disease progression in HER2+ BC patients, positioning ENPP1 as a potential prognostic marker for BrM.

Methods

Cell Culture

Human HER2+ BC cell lines JIMT-1 and SUM190 and their respective brain-tropic variants JIMT-1-BR and SUM190-BR were provided by Dr. Patricia Steeg's laboratory at the National Cancer Institute. ECs were derived from CD34+ hematopoietic stem cells isolated from human umbilical cord blood as previously described.[19] Human brain vascular pericytes (HBVP) were obtained from ScienCell Research Laboratories. Details are provided in Supplementary Materials.

Secretome Preparation

BC cell secretome (SCR) was collected after 48 hours in culture. Details are provided in Supplementary Materials

ENPP1 Knockdown

Small interfering RNA (siRNA) knockdown of ENPP1 in JIMT-1-BR and SUM190-BR cells was performed using the ON-TARGETplus Human ENPP1 siRNA SMARTpool (Dharmacon, L-003809-00-0010). Details are provided in Supplementary Materials.

ENPP1 Knockout

ENPP1 knockout (KO) JIMT-1-BR cell line was generated using two synthetic single guides RNA targeting ENPP1 and the Cas9 nuclease. The details are provided in Supplementary Materials.

In Vitro Models of the BBB

Static model.—Human CD34+ derived ECs were co-cultured with HBVP in Transwell inserts (Corning) as previously described.[20] After 6 days of co-culture, the medium in the upper compartment was replaced with 500 µL EBM-2 medium containing SCR from parental or brain-tropic cells for 24 hours. Additionally, ENPP1 Inhibitor 4e (ENPP1i; Cayman Chemical; CAY-37687) was added at 10 µM during incubation with brain-tropic cell SCR for 24 hours. BBB integrity was assessed by measuring the transendothelial flux of 4 kDa FITC-dextran and transendothelial electrical resistance (TEER) as previously described.[21] Details are provided in Supplementary Materials.

Dynamic model.—Human CD34+ derived ECs were co-cultured with HBVP using an Organ-on-a-Chip Crossflow membrane and subjected to flow via the IBIDI pump system. On day 6, the flow was stopped, and SCR derived from wild type (WT) or ENPP1-knockdown JIMT-1-BR or SUM190-BR cells was added to the apical side. Afterward, the perfusion system was changed to a smaller one, and the chip was connected to the IBIDI pump for 24 hours at a flow rate of 0.3 mL/min. BBB permeability to fluorescent 4 kDa FITC-dextran was then assessed under static conditions. Details are provided in Supplementary Materials.

Immunocytochemistry

ECs were fixed with 4% PFA (Sigma Aldrich) for 20 minutes at RT for claudin-5, zonula occludens (ZO-1), and β-catenin identification. See Supplementary Materials for details.

Animal Studies

All animal experiments were approved by the Animal Welfare Committee of the Faculty of Medicine of the University of Coimbra (ORBEA 04-2021) and by the Portuguese National Authority for Animal Health and were conducted following the European Community directive guidelines for the use of animals in the laboratory (2010/63/EU) transposed to the Portuguese law in 2013 (Decreto-Lei 113/2013).

Female outbred athymic Swiss nude (Foxn1nu/nu) mice (8–12 weeks old, 20–30 g) were divided into different groups to assess the impact of ENPP1 in pre-metastatic niche and BrM formation. See Supplementary Materials for detailed protocols.

In Vivo BBB Permeability Assessment

Following the establishment of the animal models, fluorescence imaging (FLI) was conducted 2 hours post *i.v.* injection of 20 kDa Cy7.5-dextran (3 mg/kg; Nancocs) to assess BBB permeability. See Supplementary Materials for detailed protocols.

Immunohistochemistry

Immunohistochemistry (IHC) staining was carried out on 20 µm coronal sections of OCT-embedded brain tissues according to standard protocols. See Supplementary Materials for detailed protocols.

Western Blot

Western blot was performed as described previously.[22] See Supplementary Materials for detailed protocols.

Proteomic Analysis

Proteomic analysis was conducted on 100 µg of protein using the solid-phase-enhanced sample-preparation (SP3) protocol previously described.[23] Additional details are provided in Supplementary Materials.

Kaplan–Meier Analysis

Kaplan-Meier curve was generated with RNA sequencing data from the publicly available Cancer Genome Atlas Program (TCGA) BC database with Survival-Survminer R packages. Additional details are provided in Supplementary Materials.

Statistical Analysis

All data are expressed as mean ± SEM. Graphics and statistical analysis were performed using GraphPad Prism software. Further information is provided in the Supplementary Materials.

Results

Secretome Derived From Brain-Tropic BC Cells Interferes With BBB Permeability In Vitro and In Vivo

A key step in BrM is the transmigration of cancer cells across the BBB. We hypothesized that tumor cells compromise the BBB integrity prior to the onset of metastasis, through the release of specific biomolecules. To test this hypothesis, we evaluated the effects of SCRs from HER2+ brain-tropic BC cells, JIMT-1-BR and SUM190-BR, and of their parental counterparts JIMT-1 and SUM190, within a static BBB in vitro model established by coculture of ECs with brain pericytes (Figure 1A). Exposure to the SCR from brain-tropic cells induced a significant increase in EC permeability to 4 kDa FITC-dextran (Figure 1B) and a concomitant decrease in TEER values (Figure 1C) compared to controls or their parental counterparts. This effect was paralleled by a decrease in the expression of the tight junction protein ZO-1, and the adherens junction protein β-catenin (Figure 1D–F), which are determinants for the integrity of inter-endothelial junctions within the BBB. No significant alterations were observed in the expression of these proteins in ECs exposed to the SCR of parental cells.

After identifying that tumor-secreted factors selectively disrupt the BBB, we resorted to experimental mouse models to confirm this effect in vivo. Mice received daily *i.p.* injections of SCRs ($n = 3$, per group; Figure 1G), to reproduce the continuous secretion of factors by a growing tumor for 15 days, the timeframe for PT establishment. Another group underwent orthotopic implantation of brain-tropic BC cells into the mammary fat pad for PT growth until reached a volume of 50–60 mm^3 ($n = 3$, per group; Figure 1H). We then assessed the brain vascular permeability to a systemically injected Cy7.5-dextran of 20 kDa by FLI. Fluorescent images (Figure 1I) and respective quantifications (Supplementary Figure 1A) showed an accumulation of the fluorescent dye in the brain parenchyma of mice treated with SCR from brain-tropic cells, both in vivo and ex vivo, in contrast to untreated or treated mice with SCR from the corresponding parental cell line. These observations are consistent with previous in vitro data. Notably, changes in BBB permeability resulting from daily administration of SCR closely resembled those observed in the host with the PT, suggesting a systemic tumor-mediated effect (Figure 1J and Supplementary Figure 1B). Accordingly, immunofluorescence staining of fixed brain sections revealed an increase in albumin, and a decrease in collagen IV and claudin-5 (Figure 1K and Supplementary Figure 1C) expression in the brain vessels of SCR-treated and PT-bearing mice from brain-tropic cells. These findings are indicative of severe BBB impairment, as albumin due to its large molecular weight does not cross the BBB, and collagen IV is a key protein of the basement membrane essential for endothelial support.[24] The downregulation of claudin-5, a pivotal tight junction protein, explains the loss of EC barrier integrity.[25] Overall, these results show that brain-tropic cells, but not their parental counterparts, secrete specific factors that compromise the BBB integrity early before they enter the circulation or infiltrate the brain.

Proteomic Analysis Identifies ENPP1 as a Brain Metastatic Protein

Given the similar effect of the SCR from JIMT-1-BR and SUM190-BR brain-tropic cells on the BBB, our next goal was to identify potential mediators of BBB dysfunction. We performed a mass spectrometry (MS)-based label-free quantitative proteomic analysis on the SCR derived from

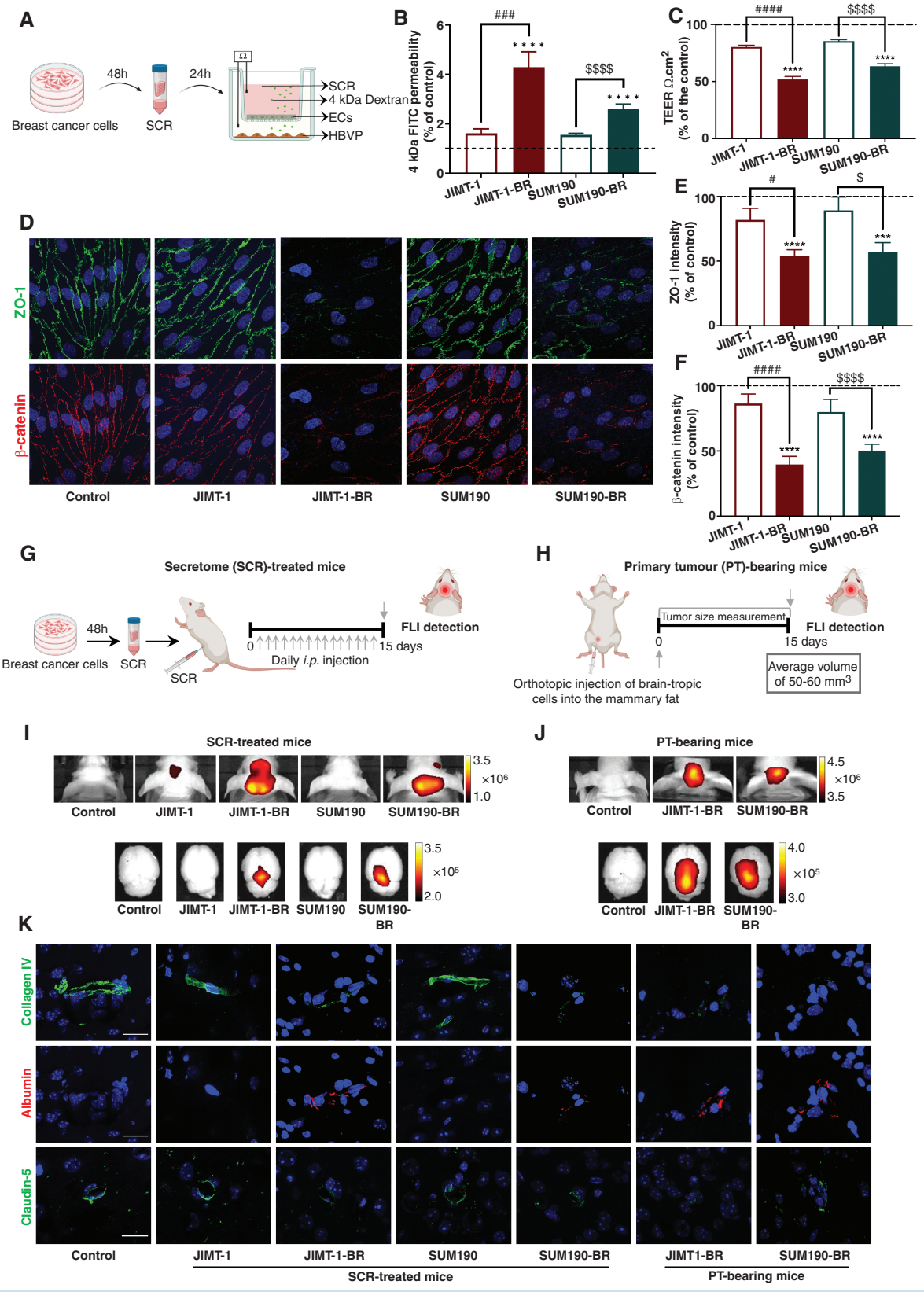

Figure 1. Secretome derived from brain-tropic breast cancer (BC) cells interferes with blood-brain barrier (BBB) permeability in vitro and in vivo (A) Scheme illustrating the establishment of a static BBB in vitro model through the co-culture of endothelial cells (ECs) with human brain vascular pericytes (HBVPs) treated with secretome (SCR) from BC cells. The BBB integrity was evaluated by measuring the (B) 4 kDa FITC-dextran permeability and (C) TEER after 24 hours of treatment, $n = 4$ to 6. (D) Representative confocal images of ZO-1 and β-catenin immunoreactivity

after BBB exposure to the SCR of BC cells. Quantification of (E) ZO-1 and (F) β-catenin immunofluorescence, $n = 4$ to 6. (G) Schematic diagram illustrating the preparation and administration schedule of the BC cell-derived SCR in mice, with mice receiving daily *i.p.* injections for 15 days, followed by assessment of BBB integrity through fluorescence imaging (FLI) detection. (H) Schematic diagram illustrating the orthotopic injection of the brain-tropic BC cells into the mammary fat pad. BBB integrity was assessed by FLI detection when the primary tumor (PT) reached a maximum volume of 50–60 mm^3. Representative FLI images of (I) SCR-treated mice ($n = 3$) and (J) PT-bearing mice ($n = 3$) in vivo (top) and ex vivo (bottom) acquired at 2 hours post-injection of 20 kDa Cy7.5-dextran. The color scale shows radiant efficiency. (K) Representative confocal images of collagen IV, albumin, and claudin-5 immunostaining in the brain vessels of SCR-treated mice (left) and PT-bearing mice (right). Statistical significance was assessed using one-way ANOVA followed by Turkey's multiple comparison test. $^{***}P < .001$, $^{****}P < .0001$ compared to control (*dashed line*). $^{\#}P < .05$, $^{\#\#\#}P < .001$, $^{\#\#\#\#}P < .0001$ compared to SCR from parental JIMT-1 cells; $^{\$}P < .05$, $^{\$\$\$\$}P < .0001$, compared to SCR from parental SUM190 cells. Nuclei were stained with Hoechst 33342. Scale Bar: 20 μm.

JIMT-1-BR and SUM190-BR cells and respective parental cell lines. A list of differentially expressed proteins (DEPs) of brain-tropic cells *vs.* parental cells was generated using an FDR-adjusted *P*-value ≤ .05. A total of 3693 proteins were identified in the SCR of the JIMT-1-BR versus JIMT-1 comparison, of which 174 were differentially expressed. For the SUM190-BR versus SUM190 comparison, we identified 240 DEPs from a total of 3567 proteins (Figure 2A). Principal component analysis (Figure 2B) and unsupervised hierarchical clustering analysis (Figure 2C) revealed distinct SCR signatures for each brain metastatic cell line compared to their respective original cell lines.

To further identify specific deregulated proteins common to JIMT-1-BR and SUM190-BR cell lines, we intersected the DEP lists from the 2 pairwise comparisons, resulting in 35 common DEPs (Figure 2D). Gene ontology (GO) enrichment analysis of these common proteins revealed involvement in various biological process terms including signal transduction, cell adhesion, cell migration, phosphatidylinositol-mediated signaling, positive regulation of cellular component movement, and the EGFR signaling pathway. Additionally, these proteins were enriched in brain-related cellular component terms, including synapses and cell-cell junctions, and molecular function terms, including integrin and receptor binding. Reactome enrichment analysis identified 6 pathways involved in extracellular matrix (ECM) degradation, ECM organization, activation of matrix metalloproteinases (MMPs), endosomal pathway, regulation of insulin-growth factor (IGF) transport, and uptake of IGF binding proteins (IGFBPs) and nuclear signaling by ERBB4 (Figure 2E). These pathways have been shown to be involved in establishing pre-metastatic niches.[26–29]

We further validated whether the identified proteins are actively secreted using *in silico* protein prediction. This validation step is important due to the potential interference from serum proteins or contamination from cell death, which are common issues when using MS-based SCR characterization.[30,31] We found that 31 out of 35 DEPs were predicted to be secreted by combining complementary information from multiple modalities (Signal P5.0, Secretome P2.0, ExoPred).[32–34] Among them, 17 proteins were classically secreted through ribosomal pathways, while the rest followed alternative secretion pathways (See Supplementary Table 1 for further details). Four proteins (PXN, OXR1, EIF1AD, PYM1) were not predicted to be secreted and were therefore excluded from further analysis.

We then performed a network analysis of the 31 common DEPs and identified four sub-clusters of functionally relevant interactions (Supplementary Figure 2A and B). Functional enrichment of the largest cluster (cluster 1) revealed top-term associations with insulin signaling and cell cycle progression, both in biological processes and molecular function annotations (Supplementary Tables 2 and 3). Notably, we identified ectonucleotide pyrophosphatase/phosphodiesterase 1 (ENPP1) as one of the query genes that consistently appeared on the enriched GO terms.

The heatmap of the 35 common DEPs, highlights ENPP1 with a higher intensity in the SCR of both JIMT-1-BR and SUM190-BR brain-tropic BC cells contrasting with the lower intensity in the corresponding parental cells (Figure 2F). ENPP1, also known as plasma cell glycoprotein 1 (PC-1), is a type II transmembrane glycoprotein with pyrophosphatase and phosphodiesterase activities.[35] This protein inhibits insulin signaling by binding to the insulin receptor (INSR) on the plasma membrane of ECs, thereby inducing insulin resistance,[13] a condition associated with BBB damage.[36,37] Given this, we point out ENPP1 as a potential mediator of BBB dysfunction, which was the focus of our further investigation.

ENPP1 Triggers BBB Dysfunction by Suppressing the AKT/GSK3β/β-Catenin Pathway in Brain ECs

First, we validated the proteomic data by measuring the protein and secreted levels of ENPP1 by BC cells using Western blot (Figure 3A) and ELISA (Figure 3B), which confirmed the high expression and secretion of ENPP1 by JIMT-1-BR and SUM190-BR cells, with negligible levels observed in their parental counterparts, thus supporting the proteomic data.

To establish the role of ENPP1 in BBB dysfunction, we exposed ECs to SCRs from BC cells in the presence of an ENPP1 inhibitor (ENPP1i; Figure 3C). Inhibition of ENPP1 effectively prevented the EC damage caused by the brain-tropic SCRs, as evidenced by the permeability and TEER (Figure 3D) values that were similar to the control conditions. In addition, it prevented the downregulation of ZO-1 and β-catenin (Figure 3E and F) further confirming the contribution of ENPP1 to BBB dysfunction.

Subsequently, we performed a complementary transmigration assay to evaluate whether these changes favored tumor cell passage through the EC monolayer. Indeed, the disruption in BBB permeability induced by the SCR facilitated the transmigration of brain-tropic cells to the lower compartment, an effect that was abolished in the presence of ENPP1i (Figure 3G). None of the parental cells crossed the BBB pretreated with the corresponding SCR, as no tumor cells were detected in the lower compartment.

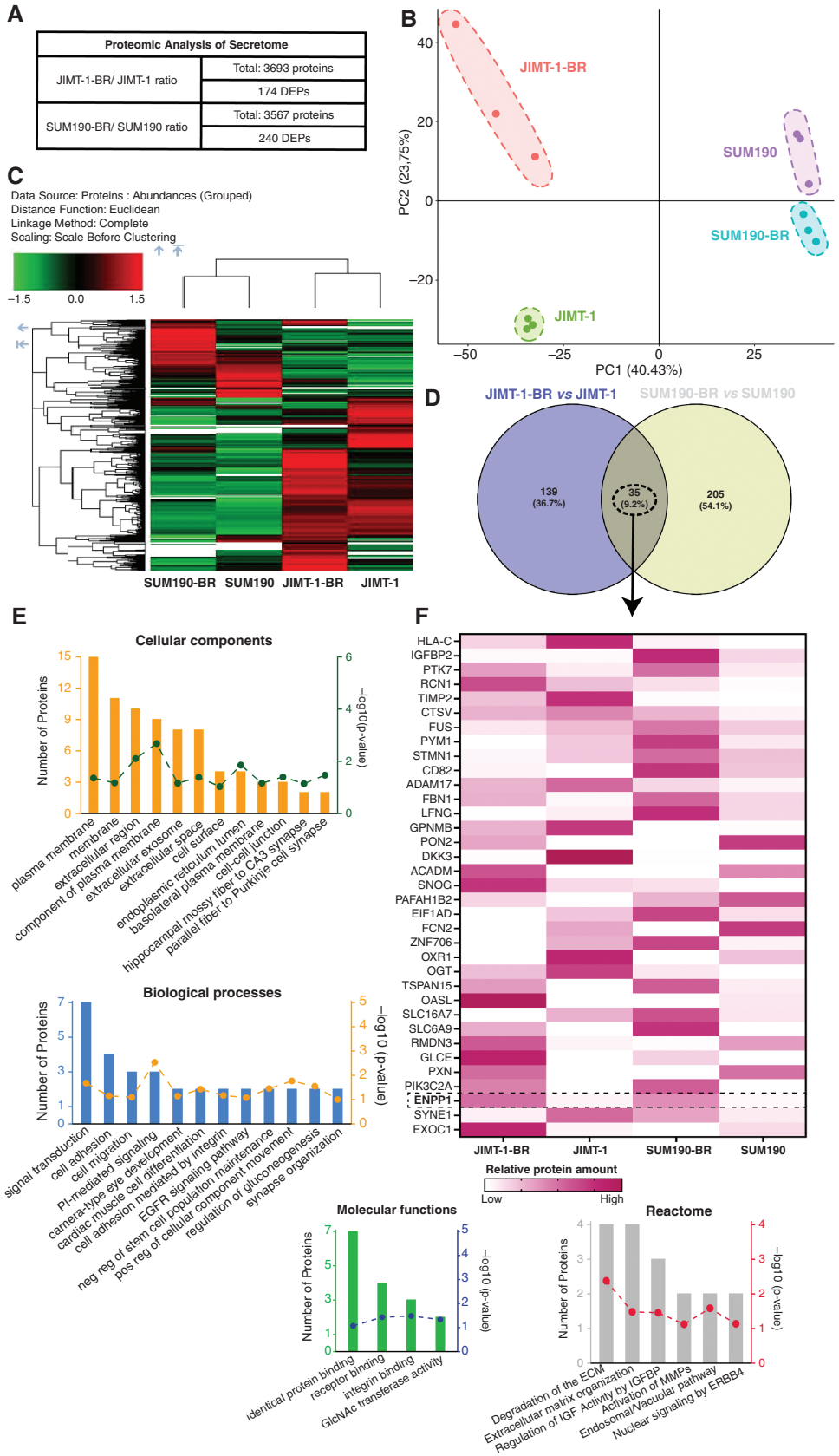

Figure 2. Proteomic analysis identifies ENPP1 as a brain metastatic protein. (A) List of total proteins and differentially expressed proteins (DEPs) between the 2 pairwise comparison groups JIMT-1-BR versus JIMT-1 and SUM190-BR versus SUM190 cells. (B) Principal component and (C)

unsupervised hierarchical clustering analysis of the SCR from breast cancer (BC) cell lines. (D) Venn diagram illustrating the overlap of DEPs identified in both comparisons, revealing common proteins in the SCR of brain-tropic cells. (E) Gene ontology analysis encompassing cellular components, biological process, and molecular functions, along with Reactome pathway enrichment analysis output of the 35 common DEPs between the 2 pairwise comparison groups. Numbers of involved proteins are indicated by the left *y*-axis and displayed as bars; *P*-values (as –Log10 values) are indicated by the right *y*-axis and displayed in dots. (F) Heatmap of protein abundance expression of the 35 common DEPs in BC cell lines.

These results confirm the importance of BBB disruption for the transmigration of BC cells and implicate ENPP1 in this process.

The insulin pathway regulates endothelial integrity by stabilizing tight junction proteins via the AKT/GSK3β pathway.[37] Activation of AKT leads to the phosphorylation of GSK3β at Ser9 and subsequent inactivation, resulting in the stabilization and accumulation of β-catenin in the cytoplasm and its translocation to the nucleus. In the nucleus, β-catenin binds to the TCF/LEF complex and regulates the expression of tight junction proteins, including ZO-1, claudin-5, and β-catenin for maintaining BBB integrity.[38–40] Since ENPP1 interacts with INSR and inhibits insulin signal transduction,[13,15] we hypothesized that ENPP1 induces BBB dysfunction by suppressing insulin signaling and its downstream AKT/GSK3β/β-catenin pathway (Figure 3H).

To test this hypothesis, we assessed downstream pathway protein expression in ECs after exposure to the SCR derived from brain-tropic JIMT-1-BR and SUM190-BR cells upon stimulation with insulin, with and without ENPP1i.

Incubation with SCR impaired the insulin pathway by decreasing the phosphorylation of INSR and reducing the phosphorylation levels of AKT and GSK3β (Figure 3I and Supplementary Figure 3A). This led to the suppression of the GSK3β/β-catenin pathway, as indicated by the decreased levels of AXIN2, a target gene of the Wnt/β-catenin pathway, as well as decreased levels of total and nuclear β-catenin (Supplementary Figure 3B). These effects were reversed by the specific ENPP1i, as demonstrated by an increase in all tested proteins to levels comparable to the control condition without SCR exposure. The only exception was AXIN2 in cells exposed to the SCR of SUM190-BR cells. This finding is consistent with the observed effects of ENPP1i in maintaining the ZO-1 and β-catenin expression in ECs (Figure 3F), further confirming the importance of INSR signaling in regulating intercellular junction integrity at the BBB.

Taken together, these results suggest that the ENPP1 in the SCR disrupts the BBB permeability by inhibiting insulin signaling and the AKT/GSK3β/β-catenin downstream pathway.

ENPP1 Knockdown in Brain Metastatic Cells Prevents BBB Dysfunction

To confirm the results obtained with the ENPP1i, we knockdown the protein in JIMT-1-BR and SUM190-BR brain-tropic cells by siRNA. The SCRs were collected for further incubation with the BBB co-culture model and preconditioning mice. Knockdown resulted in a robust reduction in ENPP1 expression in both JIMT-1-BR and SUM190-BR cells by 90% and 80%, respectively, as confirmed by western blot (Figure 4A). Non-targeting siRNA (siNT) served as a positive control for both cell lines. In this case, we used a microfluidic-based co-culture BBB model under flow-induced shear stress to mimic the dynamic physiological conditions in brain vessels. The SCRs were added to the luminal side of the BBB model for 24 hours before assessing the permeability to a 4 kDa FITC-dextran (Figure 4B). The results were consistent with those observed with the ENPP1i. The SCR from ENPP1 silencing cells had no effects on the permeability of ECs in contrast to the SCR from siNT cells (Figure 4C) that increased substantially the vascular permeability under flow conditions, confirming the contribution of ENPP1 in EC dysfunction. Moreover, the expression and distribution of the tight junction proteins claudin-5 and ZO-1, and the adherens protein β-catenin, which regulates the paracellular permeability across the BBB, were not affected by the SCR of ENPP1-silenced JIMT-1-BR and SUM190-BR cells nor by the SCR of parental JIMT-1 and SUM190 cells (Figure 4D–G).

Next, we asked whether preconditioning mice with SCR of ENPP1-silenced cells would affect the BBB permeability. Consistent with the in vitro data, ENPP1 silencing prevented BBB damage, as evidenced by the absence of the fluorescent probe in the brain of mice, which was otherwise evident in mice treated with the whole-SCR of brain metastatic cells ($n = 3$, per group; Figure 4H and Supplementary Figure 4A). Moreover, the immunostaining of brain sections confirmed the lack of albumin extravasation in the brain parenchyma and the expression of claudin-5 and collagen IV in the brain vessels of animals treated with SCR of ENPP1-silenced cells (Figure 4I and Supplementary Figure 4B), which is indicative of an intact functional BBB. Together, these results confirmed the contribution of tumor-secreted ENPP1 in vascular remodeling and EC dysfunction.

Primary Tumor Disrupts the BBB Through the Systemic Release of ENPP1

We next asked whether ENPP1 KO would affect the tumorigenicity of brain metastatic cells in vivo. Based on the consistent and similar results observed with the two brain metastatic cell lines, we performed further experiments using only the JIMT-1-BR cells. We used the CRISPR/Cas9 technology to generate ENPP1-KO JIMT-1-BR cells. The KO efficiency was confirmed by western blot, which showed a significant reduction in ENPP1 compared to the LOXP-KO control JIMT-1-BR cells (Figure 5A).

First, we evaluated whether loss of ENPP1 would affect tumor growth at the primary site. For that, WT ($n = 3$) and ENPP1-KO ($n = 3$) JIMT1-BR cells were injected orthotopically into the mammary fat pad of female mice (Figure 5B). Parental JIMT-1 cells were used for comparison ($n = 3$). Interestingly,

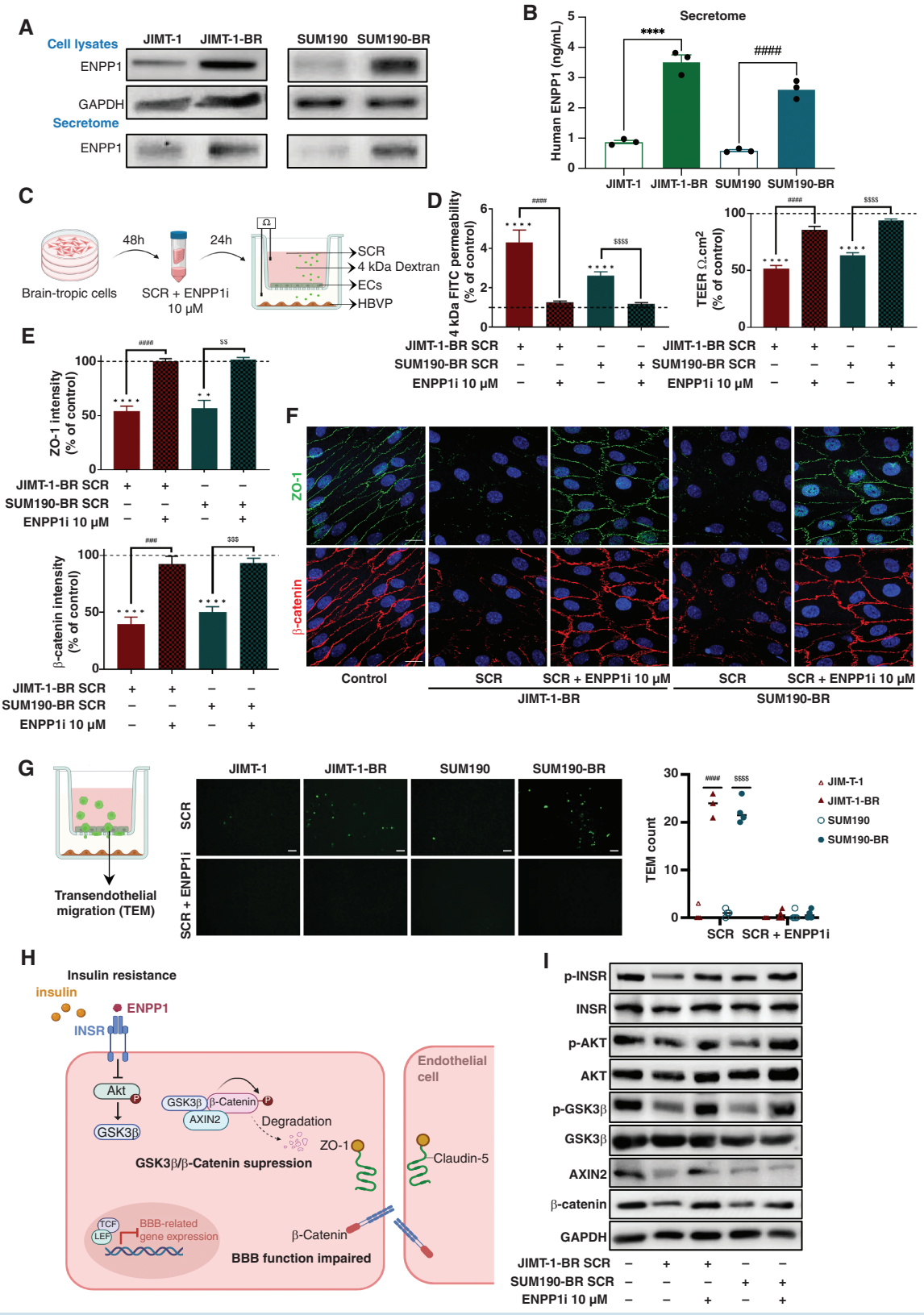

Figure 3. ENPP1 triggers blood-brain barrier (BBB) dysfunction by suppressing the AKT/GSK3β/β-catenin pathway in brain endothelial cells. (A) Representative western blot of ENPP1 expression in breast cancer (BC) cell lysates (top) and SCR (bottom). (B) ELISA analysis of ENPP1 levels in the SCR of BC cells. Statistical significance was assessed using Mann–Whitney test. $^{***}P < .001$ compared to JIMT-1-BR cells. $^{\#\#\#}P < .001$ compared to SUM190-BR cells. (C) Scheme illustrating the establishment of a static BBB in vitro model through the co-culture of endothelial cells (ECs) with HBVPs treated with SCR from brain-tropic cells in the absence or presence of the ENPP1 inhibitor (ENPP1i) at 10 μM. The BBB

integrity was evaluated by measuring the (D) 4 kDa FITC-dextran permeability and TEER after 24 hours of treatment, $n = 4$ to 6. (E) Quantification of ZO-1 and β-catenin immunofluorescence and (F) representative confocal images of ZO-1 and β-catenin immunoreactivity in ECs after treatments, $n = 4$ to 6. (G) Schematic illustration of GFP+ BC cells transmigration through the BBB after exposure to the SCR from BC cells, in the presence or absence of ENPP1i. Quantification and representative images of transendothelial migration (TEM) of BC cells across the BBB, $n = 3$. Statistical significance was assessed using Mann–Whitney test. $^{\#\#\#\#}P < .0001$ compared to JIMT-1 cells. $^{\$\$\$\$}P < .0001$ compared to SUM190 cells. Scale Bar: 100 μm (H) Schematic diagram illustrating the EC dysfunction mediated by ENPP1 by suppressing insulin signaling and downstream AKT/GSK3β/β-catenin pathway. (I) Representative images from western blot analysis of p-INSR, INSR, p-AKT, AKT, p-GSK3β, GSK3β, AXIN2, and β-catenin in ECs upon the treatment with the SCR, in the presence or absence of ENPP1i, $n = 4$ to 5. GAPDH was used as the loading control and for band density normalization. Statistical significance was assessed using one-way ANOVA followed by Turkey's multiple comparison test. $^{**}P < .01$, $^{****}P < .0001$ compared to control (*dashed line*). $^{\#\#\#\#}P < .0001$ compared to SCR from JIMT-1-BR cells; $^{\$\$}P < .01$, $^{\$\$\$}P < .001$ $^{\$\$\$\$}P < .0001$ compared to SCR from SUM190-BR cells. Nuclei were stained with Hoechst 33342. Scale Bar: 20 μm.

no significant differences were observed in the tumor growth rate between the three groups, indicating that ENPP1 is not required for in situ tumor outgrowth nor affects the proliferation rate of tumor cells (Figure 5C and D).

Regarding BBB dysfunction, depletion of ENPP1 in JIMT-1-BR cells prevented endothelial hyperpermeability, as no extravasation of 20 kDa dextran probe was visible in the brains of mice implanted with these cells in contrast to those inoculated with the WT JIMT1-BR cells (Figure 5E and F). To confirm that this was a systemic effect mediated by the PT, we measured ENPP1 levels in mouse plasma by ELISA. The results showed increased ENPP1 plasma levels in mice orthotopically implanted with WT JIMT-1-BR cells compared to those with ENPP1-KO cells, which dropped to the blood levels detected in mice with tumors derived from parental JIMT-1 cells (Figure 5G). The use of a human ENPP1 ELISA kit confirmed BC cells are the primary source of systemic ENPP1 levels.

Immunohistochemical analysis of excised tumors revealed that 90% of cells in WT JIMT-1-BR PTs stained strongly positive for ENPP1, while only 50% of cells in tumors from ENPP1-KO and parental cells showed weaker positive staining (Figure 5H), which correlates with ENPP1 plasmatic levels in mice.

These findings suggest that BC cell-derived ENPP1 is central to BBB dysfunction, but not essential for the tumor growth at the primary site.

ENPP1 Knockout Decreases the Metastatic Potential of Brain Metastatic Cells

Building on our previous findings, we investigated whether ENPP1 affects the formation of BrM. For that, we resorted to an experimental brain metastatic model by intracardiac injection on tumor cells in the left ventricle. Animals were divided into four groups and received intracardial injections of the following cells: WT JIMT-1-BR ($n = 6$), LOXP-KO JIMT-1-BR (control vector; $n = 3$), ENPP1-KO JIMT-1-BR ($n = 9$), and JIMT-1 parental cells ($n = 3$; Figure 6A). Bioluminescence imaging (BLI) confirmed the higher metastatic potential of the WT and LOXP-KO cells compared to the ENPP1-KO and JIMT-1 cells, as indicated by the faster growth rate of metastatic lesions (Figure 6B). Curiously, brain-tropic cells lacking ENPP1 showed a slow growth rate similar to that of parental cells. In particular, mice injected with WT or LOXP-KO cells developed brain metastatic lesions 7 days post-inoculation that evolved progressively to multiple foci. In contrast, the manifestation of BrM originating from ENPP1-KO cells became visible at later time points (7 days, $n = 2$; 11 days, $n = 3$; 19 days, $n = 1$; 22 days, $n = 2$) and displayed a slower progression rate similar to their original parental cell line (Figure 6C). One out of nine mice injected with ENPP1-KO cells did not develop BrM within the 50-day follow-up period.

Accordingly, ex vivo fluorescence imaging of intact mouse brains confirmed a lower number of GFP-positive brain foci in mice injected with ENPP1-KO cells and JIMT-1 compared to those injected with WT and LOXP-KO cells (Figure 6D). Histological analysis also confirmed a reduction in the metastatic foci and metastatic burden in mice injected with ENPP1-KO cells, ranging from 2 to 3 metastatic foci with a large lesion measuring 3 mm in diameter compared to those injected with the WT or LOXP-KO JIMT-1-BR cells. In the latter, the number of metastatic foci ranged from 6-9, with the large lesion reaching 12 mm in diameter (Figure 6E). This reduction is due to the decreased ability of tumor cells to extravasate across the BBB and reach the brain, as ENPP1 does not affect tumor cell proliferation.

We also assessed plasma ENPP1 levels by ELISA to evaluate whether systemic ENPP1 levels correlate with metastatic burden. In agreement with metastatic progression, higher levels of ENPP1 were found in animals with large BrM derived from both WT and LOXP-KO JIMT-1-BR cells, in contrast to those derived from ENPP1-KO JIMT-1-BR and JIMT-1 cells (Figure 6F), confirming that developing BrM is the source of systemic ENPP1. The pooled Kaplan–Meier curves showed a longer overall survival (Figure 6G) and metastasis-free survival (Figure 6H) in animals injected with ENPP1-KO cells compared to those injected with LOXP-KO cells. Additionally, we found that lower levels of ENPP1 correlated with longer survival (Figure 6I), further confirming the functional role of ENPP1 in promoting BrM formation.

In a pilot study to explore the potential benefit of targeting ENPP1, animals were treated daily with ENPP1i (2 mg/kg) following intracardiac cell inoculation. This schedule prevented the formation of BrM in 60% of the animals (3 out of 5) and delayed progression in the remaining two (Figure 6J), as confirmed by histologic examination (Figure 6K). All vehicle-treated animals (3 out of 3) formed multiple BrM by day 7 that progressed and reached the human endpoints by days 28–30, at which point we concluded the study. At that time, none of the ENPP1i-treated animals had reached humane endpoints, and all were alive, raising the possibility of a therapeutic benefit from targeting ENPP1 to prevent BrM.

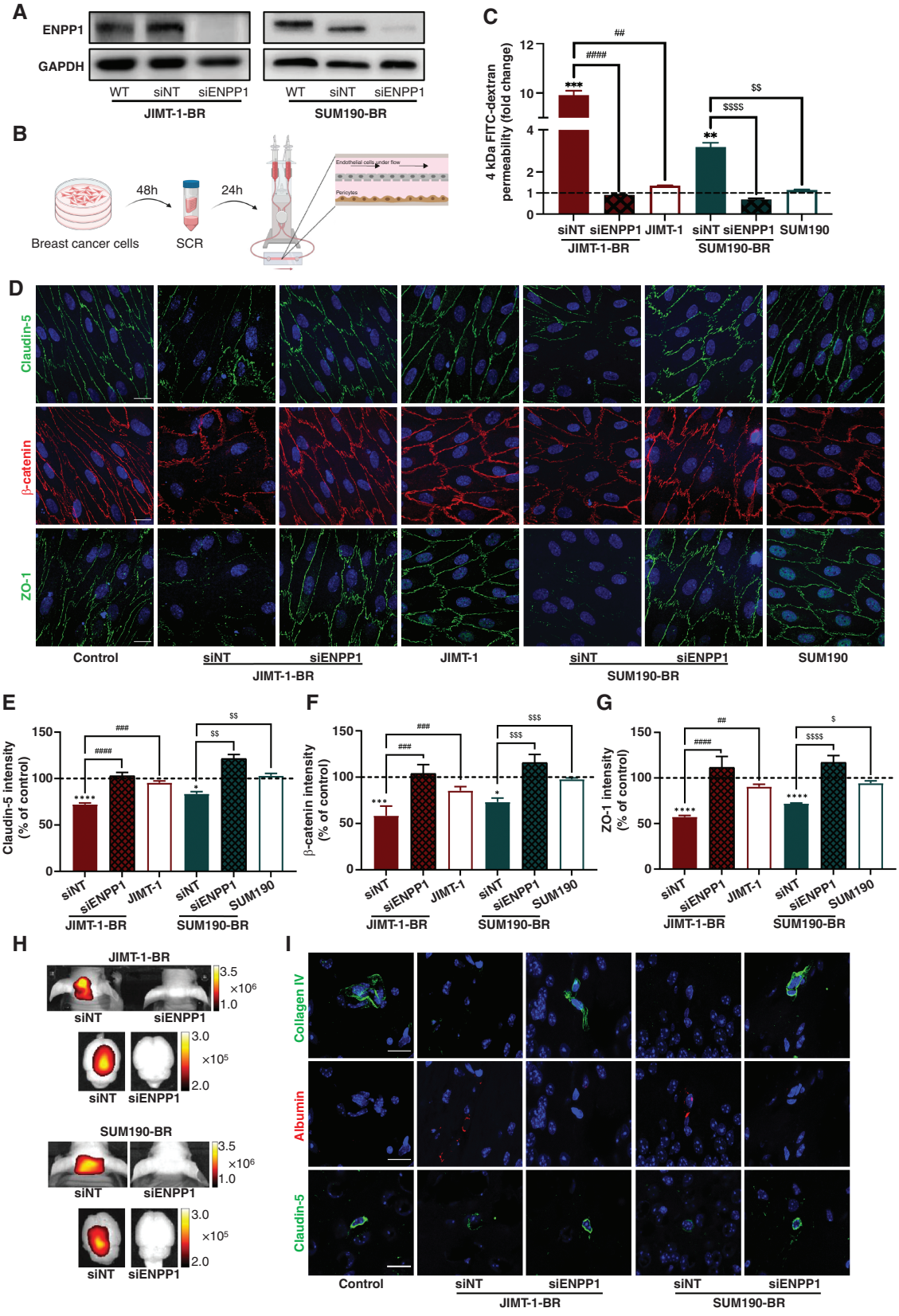

Figure 4. ENPP1 knockdown in brain metastatic cells prevents blood-brain barrier (BBB) dysfunction. (A) Representative western blot of ENPP1 expression in wild type (WT), non-targeting siRNA (siNT) and ENPP1 siRNA knockdown (siENPP1) in JIMT-1-BR (left) and SUM190-BR (right) brain metastatic cells. (B) Scheme of the microfluidic-based BBB in vitro model established by the co-culture of endothelial cells (ECs) with HBVPs under flow conditions treated with SCR from parental cells, siENPP1, and siNT brain-tropic cells. The BBB integrity was evaluated by measuring the (C) 4 kDa FITC-dextran permeability, $n = 3$. (D) Representative confocal images of claudin-5, β-catenin, ZO-1 immunoreactivity.

Quantification of immunofluorescence levels of (E) claudin-5, (F) β-catenin, and (G) ZO-1 proteins in ECs. (H) Representative FLI images of in vivo and ex vivo SCR-treated mice acquired at 2h post-injection of 20 kDa Cy7.5-dextran, $n = 3$ per group. The color scale shows radiant efficiency. (I) Representative confocal images of collagen IV, albumin, and claudin-5 immunostaining in the brain vessels. Statistical significance was assessed using one-way ANOVA followed by Dunn's multiple comparison test. $^{*}P < .05$, $^{**}P < .01$, $^{***}P < .001$, $^{****}P < .0001$ compared to control (*dashed line*). $^{\#\#}P < .01$, $^{\#\#\#}P < .001$, $^{\#\#\#\#}P < .0001$ compared to SCR from siNT JIMT-1-BR cells; $^{\$}P < .05$, $^{\$\$}P < .01$ $^{\$\$\$}P < .001$, $^{\$\$\$\$}P < .0001$ compared to SCR from siNT SUM190-BR cells. Nuclei were stained with Hoechst 33342. Scale Bar: 20 µm.

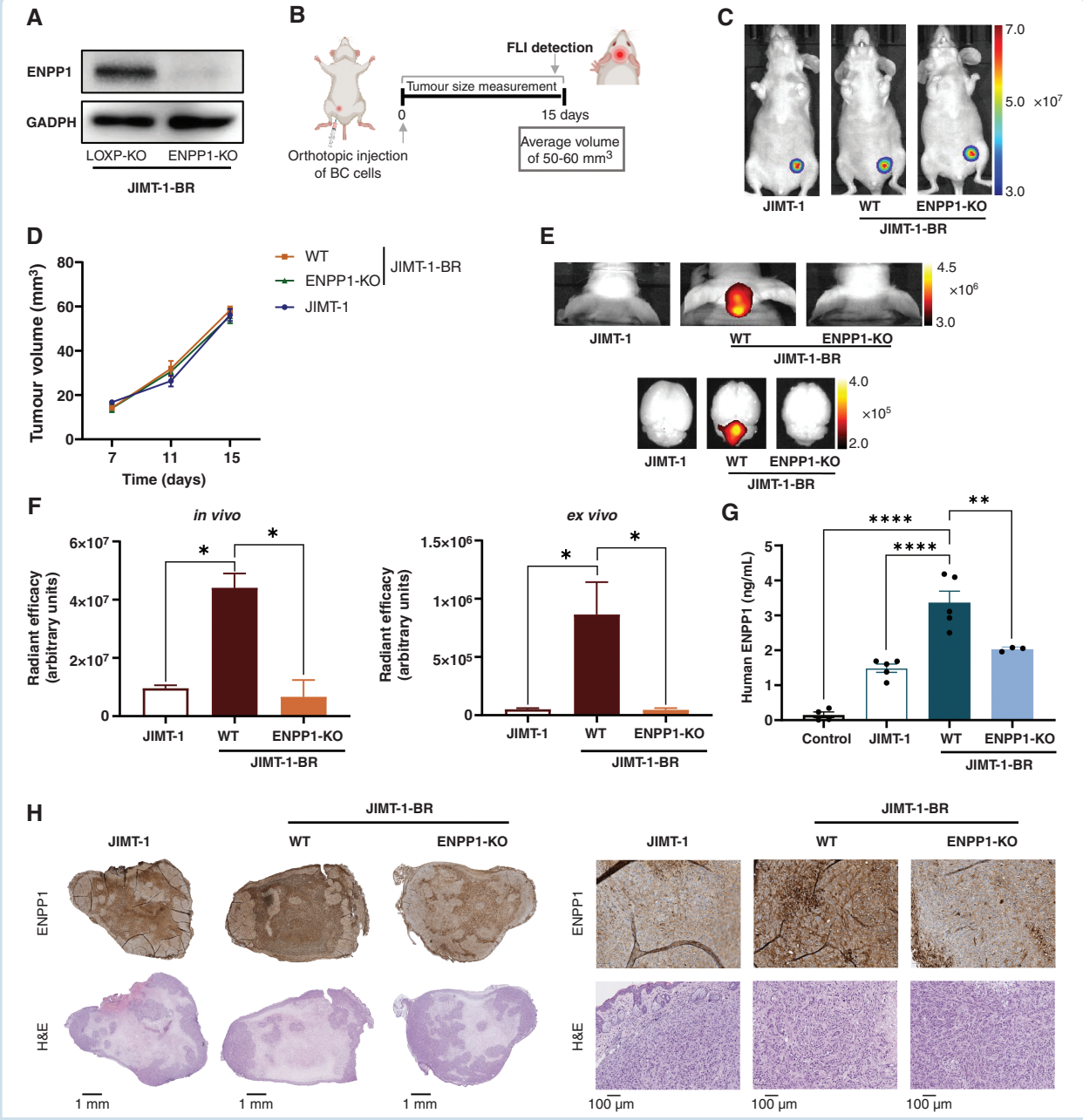

Figure 5. Primary tumor (PT) disrupts the blood-brain barrier (BBB) through the systemic release of ENPP1. (A) Representative western blot of ENPP1 expression in LOXP (control vector) and ENPP1 knockout (KO) JIMT-1-BR cells. (B) Schematic diagram illustrating the orthotopic injection of JIMT-1-BR (WT and ENPP1-KO) and parental JIMT-1 cells into the mammary fat pad. BBB integrity was assessed by FLI detection when the PT reached a maximum volume of 50–60 mm^3, $n = 3$ per group. (C) Representative BLI images of PT 15 days after the implementation of breast cancer (BC) cells. The color scale shows radiance (photons/sec/cm^2/sr). (D) Volumes of orthotopic primary breast tumors over time. (E) Representative FLI images and (F) quantification of fluorescence in PT-bearing mice in vivo (left) and ex vivo (right) 2 hours post-injection of 20 kDa Cy7.5-dextran. The color scale shows radiant efficiency. (G) Plasma levels of ENPP1 in healthy mice and mice bearing PTs from JIMT-1, WT JIMT-1-BR, and ENPP1-KO JIMT-1-BR cells. (H) Representative immunohistochemical images of ENPP1 expression (top) and histopathological H&E (bottom) in resected PTs. Scale bars: 1 mm (left) and 100 µm (right). Statistical significance was assessed using one-way ANOVA followed by Dunn's multiple comparison test. $^{*}P < .05$, $^{**}P < .01$, $^{****}P < .0001$ compared to WT JIMT-1-BR PT-bearing mice.

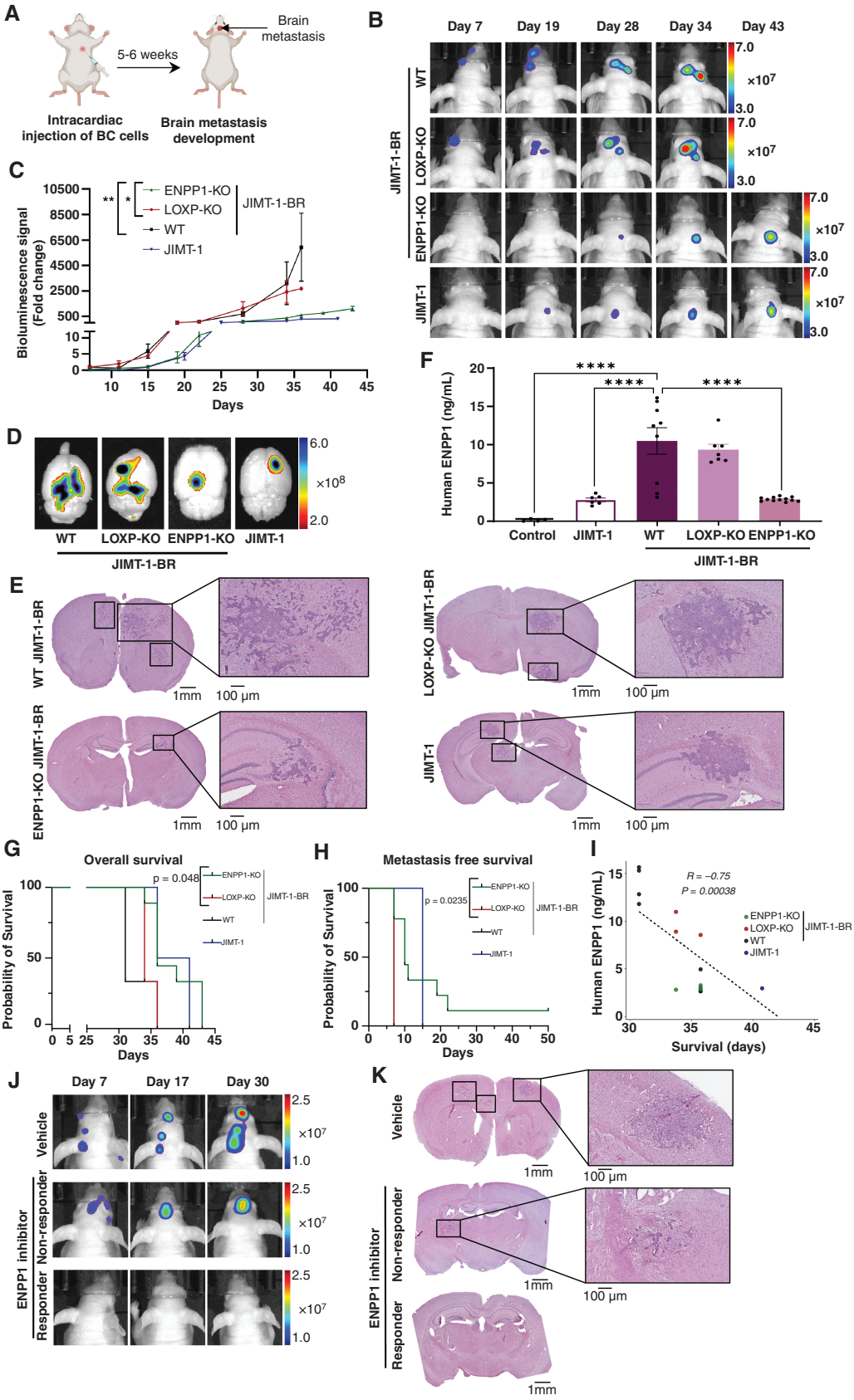

Figure 6. ENPP1 knockout decreases the metastatic potential of brain metastatic cells. (A) Scheme of the experimental model of BrM established by intracardiac injection of parental JIMT-1 ($n = 3$) and JIMT-1-BR WT ($n = 6$), LOXP-KO ($n = 6$), and ENPP1-KO ($n = 9$) cells into the left ventricle. (B) Representative BLI images of experimental BrM formation over time post-intracardiac injection of breast cancer (BC) cells. The

color scale shows radiance (photons/sec/cm^2/sr) (C) Quantification of BLI signal intensities over time (fold change from day 0 BLI measurement). Statistical significance was assessed using two-way ANOVA followed by Turkey's multiple comparison test. $^*P < .05$, $^{**}P < .01$ compared to ENPP1-KO JIMT-1-BR BrM-bearing mice. (D) Ex vivo imaging of GFP+ BC cells in the brain. The color scale shows radiant efficiency. (E) Representative images of histopathological H&E of whole brain sections showing the number and size of BrMs. Scale bars: 1 mm, in inserts: 250 µm. (F) Plasma levels of ENPP1 in healthy mice and mice bearing BrM from JIMT-1, WT JIMT-1-BR, LOXP-KO JIMT-1-BR, and ENPP1-KO JIMT-1-BR cells. Statistical significance was assessed using one-way ANOVA followed by Turkey's multiple comparison test. $^{****}P < .0001$ compared to WT JIMT-1 BrM-bearing mice. Survival analysis by Kaplan–Meier showed a significantly shortened (G) overall survival ($P = .048$) and (H) metastasis-free survival ($P = 0.0235$) for mice bearing BrM from ENPP1-KO compared to LOXP-KO. Statistical significance was assessed using log-rank test. (I) Two-sided Pearson correlation was assessed between ENPP1 plasma levels and overall survival of mice. (J) Representative BLI images showing the progression of BrM formation over time in mice treated with an ENPP1 inhibitor ($n = 5$) or vehicle ($n = 3$). The color scale shows radiance (photons/sec/cm^2/sr). (K) Representative images of histopathological H&E of whole brain sections showing brain metastatic foci. Scale bars: 1 mm, in inserts: 250 µm.

We also investigated whether ENPP1 is required for BC cells' survival and outgrowth in the brain environment. However, direct intracranial injections of WT and ENPP1-KO cells showed no differences in BrM progression rate between animal groups (Supplementary Figure 5A and B). These findings confirm that ENPP1 is essential for the early stage of BC cell extravasation across the BBB, but not for in situ brain outgrowth.

Additionally, we evaluated the clinical significance of ENPP1 as a predictive biomarker of metastasis using data from over 289 patients in the TCGA database. Kaplan–Meier analysis revealed that high levels of ENPP1 expression in PT samples of HER2+ BC patients were associated with faster metastatic/disease progression (Supplementary Figure 6), which emphasizes the role of ENPP1 in promoting metastatic progression in human HER2+ BC.

Collectively, these data position systemic ENPP1 as a primary driver of BBB dysfunction and a facilitator of BrM in HER2+ BC patients.

Discussion

Transmigration across the BBB is a rate-limiting step for overt colonization of metastatic cells in the brain.[7] Understanding how tumor cells evolve to overcome this barrier is essential for developing targeted therapeutic strategies to prevent or treat BrM. Our study uncovered a novel mechanism, by which HER2+ BC cells compromise BBB integrity to metastasize to the brain. We identified ENPP1, a type II transmembrane glycoprotein with nucleotide pyrophosphatase/phosphodiesterase enzymatic activity,[35] specifically enriched in the SCR of HER2+ brain metastatic cell lines and also in the plasma of tumor-bearing mice with a severely compromised BBB, allowing the extravasation of a 20 kDa dextran, which under physiological conditions excludes molecules larger than 0.4 kDa.[41] Recent studies have implicated ENPP1 in restraining anti-tumor immunity by inhibiting the cGAS/cGAMP/STING pathway and driving immunosuppression in the tumor microenvironment while promoting tumor progression and metastasis.[42–44]

Our study reveals a novel function for ENPP1 in the dysregulation of tight junction proteins in brain ECs via suppression of the insulin signaling and the downstream AKT/GSK3β/β-catenin pathway. Previous studies have shown that ENPP1 negatively modulates INSR signaling, contributing to the development of insulin resistance,[12–16] a condition associated with BBB dysfunction in several pathological conditions such as type 2 diabetes,[18,45] bipolar disorders,[46] and Alzheimer's disease.[17] Ito et al. confirmed the physiological importance of INSR signaling in regulating the integrity of tight junction proteins in brain ECs. They found that impaired insulin signaling by hyperglycemia reduced the integrity of the tight junction proteins ZO-1 and claudin-5 in hCMEC/D3 cells, an effect they attributed to inactivation of GSK3β phosphorylation downstream of PI3K/AKT inhibition.[37] Our data suggest a similar mechanism, as we also observed the downregulation of tight and adherens junction proteins in both static and dynamic BBB models exposed to the SCR and its reversal with genetic knockdown or ENPP1 pharmacological inhibition. The reactivation of the AKT/GSK3β mediated Wnt/β-catenin pathway observed with the ENPP1i supports this hypothesis. The fact that ENPP1 was barely detected in the SCR of parental cells, with limited metastatic potential, suggests that it is a specific molecular feature evolved by brain metastatic cells to overcome the BBB.

We showed that ENPP1 genetic ablation impaired the brain metastatic ability of brain-tropic cells but not in situ brain outgrowth in the intracranial model, suggesting that ENPP1 is not oncogenic per se. Similarly, ENPP1-KO does not affect the PT growth in the mammary fat pad but effectively prevents BBB damage, underscoring the pivotal role of ENPP1 in early EC dysfunction preceding brain colonization. Importantly, ENPP1 pharmacological inhibition abolished metastasis formation in 60% of the animals, highlighting the potential of ENPP1-targeted therapies to delay or prevent BrM. Furthermore, we found that ENPP1 levels correlated with metastatic burden and inversely with overall survival, suggesting that systemic ENPP1 has both a functional role in instigating BBB dysfunction and a prognostic value for BrM risk. A recent study by Li et al. has found high ENPP1 expression in matched primary and metastatic clinical samples from various tumors, including BC, with BrM having the highest ENPP1 expression levels among metastatic sites.[42] They reasoned that ENPP1 overexpression is associated with poor prognosis related to its function as a negative regulator of cGAS/cGAMP/STING signaling and immunosuppression. We measured cGAMP levels in brain-tropic cell SCR and observed a significant increase upon ENPP1 knockdown, similar to that observed in parental cells. Likewise, in mice bearing PT or BrM, we found increased plasma cGAMP levels following ENPP1 KO (Supplementary Figure 7A–C). These findings

suggest that ENPP1-regulated extracellular cGAMP is present in our model, and may be involved in BBB dysfunction during premetastatic stage, which needs to be elucidated in future studies. It is also worth mentioning that we did not confirm the STING pathway inactivation and immune evasion, as this was beyond the scope of this study. Addressing this issue would require a mouse model with an intact immune system, which is not the case in our model.

Consistently, Kaplan–Meier survival analysis using data from the TCGA database showed that HER2+ BC patients with high ENPP1 expression in the PT had shorter disease-free and distant metastasis-free intervals, suggesting a clear association with a rapid metastatic progression. These findings encouraged further prospective cohort studies to determine whether plasmatic ENPP1 can be used as a predictive biomarker for BrM relapse in HER2+ BC patients. While this study was focused on HER2+ BC, our findings could potentially be generalized to other tumors with a propensity to spread to the brain and should be investigated.

In summary, we demonstrated for the first time that tumor-secreted ENPP1 systemically increases the BBB permeability by tight and adherens junction protein disruption and promotes the formation of BrM. Additionally, we highlight ENPP1's potential as a biomarker for early-stage BrM, as its secretion by HER2+ breast tumors precedes the onset of BrM.

The functional and prognostic implications of ENPP1 that we have identified suggest that targeting ENPP1 may be an effective therapeutic strategy to prevent or inhibit BrM relapse in HER2+ BC. ENPP1 has recently gained attention as a therapeutic target for immunotherapy, and several clinical trials are currently underway in patients with advanced solid tumors.[47,48] Our findings lay the groundwork for exploring the use of ENPP1 inhibitors as a strategy for preventing BrM.

Supplementary material

Supplementary material is available online at *Neuro-Oncology* (https://academic.oup.com/neuro-oncology).

Keywords

BBB dysfunction | brain metastasis | ENPP1 | HER2-positive breast cancer | secretome

Funding

This work was supported by the Portuguese Foundation for Science and Technology (FCT) through the PROJECT PTDC/BTM-SAL/4451/2020 and STRATEGIC PROJECTS (UIDB/04539/2020 and UIDP/04539/2020). L.S. is a Ph.D. fellow of the FCT (PD/BDE/150707/2020). F. T. is a Ph.D. fellow of the FCT (2021.06297.BD).

Conflict of interest statement

None declared.

Authorship statement

L.S., F.T., H.F., S.A., and E.C. performed experiments, acquisition, analysis and interpretation of data. J.S., P.T., and R.A. performed experiments. H.F. and E.C. performed bioinformatics analysis. A.S.R. performed proteomic analysis. J.N.M., A.P.S., L.F., and A.J.A. assisted with data analysis. L.S. wrote the manuscript. C.M.G. designed and supervised the study revised the manuscript and obtained financial support. All authors reviewed the manuscript and approved its content.

Data availability

The mass spectrometry proteomics data have been deposited to the ProteomeXchange Consortium via the PRIDE partner repository with the dataset identifier PXD051579.

Affiliations

Institute for Nuclear Sciences Applied to Health (ICNAS) and Coimbra Institute for Biomedical Imaging and Translational Research (CIBIT), University of Coimbra, Coimbra, Portugal (L.S., S.F.F.A., J.S., A.J.A.); Faculty of Medicine, Institute of Pharmacology and Experimental Therapeutics, Coimbra Institute for Clinical and Biomedical Research (iCBR), University of Coimbra, Coimbra, Portugal (L.S., H.R.S.F., S.F.F.A., E.C., A.P.S., C.M.G.); Center for Neuroscience and Cell Biology (CNC-UC), University of Coimbra, Coimbra, Portugal (F.T., J.N.M., L.F.); Institute of Interdisciplinary Research, University of Coimbra, Coimbra, Portugal (F.T.); Center for Innovative Biomedicine and Biotechnology Consortium (CIBB), University of Coimbra, Coimbra, Portugal (F.T., H.R.S.F., E.C., J.N.M., A.P.S., L.F., C.M.G.); Clinical Academic Center of Coimbra (CACC), Coimbra, Portugal (H.R.S.F., E.C., A.P.S., C.M.G.); Pathology Department, Centro Hospitalar e Universitário de Coimbra, Coimbra, Portugal (R.A., P.T.); Cancer Metastasis Group, Instituto de Investigação e Inovação em Saúde (i3S), Porto, Portugal (A.S.R.); Faculty of Pharmacy, University of Coimbra, Coimbra, Portugal (J.N.M.)

References

1. Nayak L, Lee EQ, Wen PY. Epidemiology of brain metastases. *Curr Oncol Rep*. 2012;14(1):48–54.
2. Heitz F, Rochon J, Harter P, et al. Cerebral metastases in metastatic breast cancer: Disease-specific risk factors and survival. *Ann Oncol*. 2011;22(7):1571–1581.

3. Hackshaw MD, Danysh HE, Henderson M, et al. Prognostic factors of brain metastasis and survival among HER2-positive metastatic breast cancer patients: A systematic literature review. *BMC Cancer.* 2021;21(1):967.
4. Riggio AI, Varley KE, Welm AL. The lingering mysteries of metastatic recurrence in breast cancer. *Br J Cancer.* 2021;124(1):13–26.
5. Carvalho R, Paredes J, Ribeiro A. Impact of breast cancer cells secretome on the brain metastatic niche remodeling. *Semin Cell Dev Biol.* 2020;60:294–301.
6. Adler O, Zait Y, Cohen N, et al. Reciprocal interactions between innate immune cells and astrocytes facilitate neuroinflammation and brain metastasis via lipocalin-2. *Nature Cancer.* 2023;4(3):401–418.
7. Arvanitis CD, Ferraro GB, Jain RK. The blood–brain barrier and blood–tumour barrier in brain tumours and metastases. *Nat Rev Cancer.* 2020;20(1):26–41.
8. Chow BW, Gu C. The molecular constituents of the blood–brain barrier. *Trends Neurosci.* 2015;38(10):598–608.
9. Tominaga N, Kosaka N, Ono M, et al. Brain metastatic cancer cells release microRNA-181c-containing extracellular vesicles capable of destructing blood–brain barrier. *Nat Commun.* 2015;6(1):6716.
10. Lu Y, Chen L, Li L, Cao Y. Exosomes derived from brain metastatic breast cancer cells destroy the blood-brain barrier by carrying lncRNA GS1-600G8. 5. *Biomed Res Int.* 2020;2020(1):1–10.
11. Wang S, Böhnert V, Joseph AJ, et al. ENPP1 is an innate immune checkpoint of the anticancer cGAMP–STING pathway in breast cancer. *Proc Natl Acad Sci USA.* 2023;120(52):e2313693120.
12. Xia J, Yang Y, Yang Z, Wu G, Yang J. *ENPP1 Is Correlated With Insulin Resistance and Lipid Molecules in PCOS Rats.* 2021.
13. Tassone EJ, Cimellaro A, Perticone M, et al. Uric acid impairs insulin signaling by promoting Enpp1 binding to insulin receptor in human umbilical vein endothelial cells. *Front Endocrinol.* 2018;9:98.
14. Pan W, Chandalia M, Abate N. New insights into the role of ENPP1 in insulin resistance. *J Metabonomics Metab.* 2012;1(1):10.4172/2325-9736.1000e103.
15. Goldfine ID, Maddux BA, Youngren JF, et al. The role of membrane glycoprotein plasma cell antigen 1/ectonucleotide pyrophosphatase phosphodiesterase 1 in the pathogenesis of insulin resistance and related abnormalities. *Endocr Rev.* 2008;29(1):62–75.
16. Abate N, Chandalia M, Di Paola R, et al. Mechanisms of disease: Ectonucleotide pyrophosphatase phosphodiesterase 1 as a'gatekeeper'of insulin receptors. *Nat Clin Pract Endocrinol Metab.* 2006;2(12):694–701.
17. Wang Z, Tang X, Swaminathan SK, Kandimalla KK, Kalari KR. Mapping the dynamics of insulin-responsive pathways in the blood–brain barrier endothelium using time-series transcriptomics data. *NPJ Syst Biol Appl.* 2022;8(1):29.
18. Rask-Madsen C, King GL. Mechanisms of disease: Endothelial dysfunction in insulin resistance and diabetes. *Nat Clin Pract Endocrinol Metab.* 2007;3(1):46–56.
19. Pedroso DC, Tellechea A, Moura L, et al. Improved survival, vascular differentiation and wound healing potential of stem cells co-cultured with endothelial cells. *PLoS One.* 2011;6(1):e16114.
20. Cecchelli R, Aday S, Sevin E, et al. A stable and reproducible human blood-brain barrier model derived from hematopoietic stem cells. *PLoS One.* 2014;9(6):e99733.
21. Coelho-Santos V, Socodato R, Portugal C, et al. Methylphenidate-triggered ROS generation promotes caveolae-mediated transcytosis via Rac1 signaling and c-Src-dependent caveolin-1 phosphorylation in human brain endothelial cells. *Cell Mol Life Sci.* 2016;73(24):4701–4716.
22. Almeida SF, Santos L, Sampaio-Ribeiro G, et al. Unveiling the role of osteosarcoma-derived secretome in premetastatic lung remodelling. *J Exp Clin Cancer Res.* 2023;42(1):328.
23. Hughes CS, Moggridge S, Müller T, et al. Single-pot, solid-phase-enhanced sample preparation for proteomics experiments. *Nat Protocols.* 2019;14(1):68–85.
24. Coelho-Santos V, Leitão RA, Cardoso FL, et al. The TNF-α/Nf-κ B signaling pathway has a key role in methamphetamine–induced blood–brain barrier dysfunction. *J Cereb Blood Flow Metab.* 2015;35(8):1260–1271.
25. Jia W, Lu R, Martin TA, Jiang WG. The role of claudin-5 in blood-brain barrier (BBB) and brain metastases. *Mol Med Rep.* 2014;9(3):779–785.
26. Høye AM, Erler JT. Structural ECM components in the premetastatic and metastatic niche. *Am J Physiol Cell Physiol.* 2016;310(11):C955–C967.
27. Lobb RJ, Lima LG, Möller A. Exosomes: Key mediators of metastasis and pre-metastatic niche formation. *Semin Cell Dev Biol.* 2017;67:3–10.
28. Belfiore A, Rapicavoli RV, Le Moli R, et al. IGF2: A role in metastasis and tumor evasion from immune surveillance? *Biomed.* 2023;11(1):229.
29. Li X, Huang Q, Wang S, et al. HER4 promotes the growth and metastasis of osteosarcoma via the PI3K/AKT pathway. *Acta Biochim Biophys Sin.* 2020;52(4):345–362.
30. Brandi J, Manfredi M, Speziali G, Gosetti F, Marengo E, Cecconi D. Proteomic approaches to decipher cancer cell secretome. *Semin Cell Dev Biol.* 2018;78:93–101.
31. Caccia D, Dugo M, Callari M, Bongarzone I. Bioinformatics tools for secretome analysis. *Biochim Biophys Acta.* 2013;1834(11):2442–2453.
32. Almagro Armenteros JJ, Tsirigos KD, Sønderby CK, et al. SignalP 5.0 improves signal peptide predictions using deep neural networks. *Nat Biotechnol.* 2019;37(4):420–423.
33. Bendtsen JD, Kiemer L, Fausbøll A, Brunak S. Non-classical protein secretion in bacteria. *BMC Microbiol.* 2005;5(1):1–13.
34. Ras-Carmona A, Gomez-Perosanz M, Reche PA. Prediction of unconventional protein secretion by exosomes. *BMC Bioinf.* 2021;22(1):333.
35. Onyedibe KI, Wang M, Sintim HO. ENPP1, an old enzyme with new functions, and small molecule inhibitors—a STING in the tale of ENPP1. *Molecules.* 2019;24(22):4192.
36. Nagano H, Ito S, Masuda T, Ohtsuki S. Effect of insulin receptor-knockdown on the expression levels of blood–brain barrier functional proteins in human brain microvascular endothelial cells. *Pharm Res.* 2022;39(7):1561–1574.
37. Ito S, Yanai M, Yamaguchi S, Couraud P-O, Ohtsuki S. Regulation of tight-junction integrity by insulin in an in vitro model of human blood–brain barrier. *J Pharm Sci.* 2017;106(9):2599–2605.
38. Ramirez SH, Fan S, Dykstra H, et al. Inhibition of glycogen synthase kinase 3β promotes tight junction stability in brain endothelial cells by half-life extension of occludin and claudin-5. *PLoS One.* 2013;8(2):e55972.
39. Fei Y-x, Zhu J-p, Zhao B, et al. XQ-1H regulates Wnt/GSK3β/β-catenin pathway and ameliorates the integrity of blood brain barrier in mice with acute ischemic stroke. *Brain Res Bull.* 2020;164:269–288.
40. Liao Z, Zhou X, Li S, et al. Activation of the AKT/GSK-3β/β-catenin pathway via photobiomodulation therapy promotes neural stem cell proliferation in neonatal rat models of hypoxic-ischemic brain damage. *Ann Transl Med.* 2022;10(2):55–55.
41. Pandit R, Chen L, Götz J. The blood-brain barrier: Physiology and strategies for drug delivery. *Adv Drug Deliv Rev.* 2020;165-166:1–14.
42. Li J, Duran MA, Dhanota N, et al. Metastasis and immune evasion from extracellular cGAMP hydrolysis. *Cancer Discov.* 2021;11(5):1212–1227.
43. Carozza JA, Cordova AF, Brown JA, et al. ENPP1's regulation of extracellular cGAMP is a ubiquitous mechanism of attenuating STING signaling. *Proc Natl Acad Sci USA.* 2022;119(21):e2119189119.
44. Attalla SS, Boucher J, Proud H, et al. HER2Δ 16 Engages ENPP1 to promote an immune cold microenvironment in breast cancer. *Cancer Immunol Res.* 2023;11(9):1184–1202.
45. Roberts AC, Porter KE. Cellular and molecular mechanisms of endothelial dysfunction in diabetes. *Diab Vasc Dis Res.* 2013;10(6):472–482.

46. Calkin C, McClelland C, Cairns K, Kamintsky L, Friedman A. Insulin resistance and blood-brain barrier dysfunction underlie neuroprogression in bipolar disorder. *Front Psychiatry.* 2021;12:636174.
47. Marron T, Misleh J, Wainberg Z, et al. 1025MO Preliminary safety, pharmacokinetics and immunomodulatory activity of RBS2418, an oral ENPP1 inhibitor, alone and in combination with pembrolizumab in patients with solid tumors. *Ann Oncol.* 2023;34:S623–S624.
48. Guan D, Fang L, Feng M, et al. Ecto-nucleotide pyrophosphatase/phosphodiesterase 1 inhibitors: Research progress and prospects. *Eur J Med Chem.* 2024;267:116211.